Available online at www.sciencedirect.com

ScienceDirect

Green Energy & Environment xxx (xxxx) xxx

www.keaipublishing.com/gee

Research paper

Facile synthesis of accordion-like porous carbon from waste PET bottles-based MIL-53(Al) and its application for high-performance Zn-ion capacitor

Jiaxin Li [a], Shuai Zhang [a], Yumeng Hua [b], Yichao Lin [c], Xin Wen [a,d,*], Ewa Mijowska [a], Tao Tang [b,*], Xuecheng Chen [a,*], Rodney S. Ruoff [e,f,g,h]

[a] Faculty of Chemical Technology and Engineering, West Pomeranian University of Technology, Piastów Ave. 42, 71-065, Szczecin, Poland
[b] Key State Key Laboratory of Polymer Physics and Chemistry, Changchun Institute of Applied Chemistry, Chinese Academy of Sciences, Changchun, 130022, China
[c] School of Safety Engineering, China University of Mining and Technology, Xuzhou, 221116, China
[d] Institute of Advanced Electrical Materials, Qingdao University of Science and Technology, Qingdao, 266042, China
[e] Institute for Basic Science Center for Multiple Dimensional Carbon Materials, Ulsan, 44919, Republic of Korea
[f] Department of Chemistry, Ulsan National Institute of Science and Technology (UNIST), Ulsan, 44919, Republic of Korea
[g] Department of Materials Science and Engineering, Ulsan National Institute of Science and Technology (UNIST), Ulsan, 44919, Republic of Korea
[h] School of Energy and Chemical Engineering, Ulsan National Institute of Science and Technology (UNIST), Ulsan, 44919, Republic of Korea

Received 3 November 2022; revised 23 December 2022; accepted 3 January 2023
Available online ■ ■ ■

Abstract

It is of great scientific and economic value to recycle waste poly (ethylene terephthalate) (PET) into high-value PET-based metal organic frameworks (MOFs) and further convert it into porous carbon for green energy storage applications. In the present study, a facile and cost-effective hydrothermal process was developed to direct recycle waste PET bottles into MIL-53(Al) with a 100% conversation, then the MOF-derived porous carbon was assembled into electrodes for high-performance supercapacitors. The results indicated that the as-synthesized carbon exhibited high SSA of 1712 $m^2\ g^{-1}$ and unique accordion-like structure with hierarchical porosity. Benefit to these advantageous characters, the assembled three-electrode supercapacitor displayed high specific capacitances of 391 F g^{-1} at the current density of 0.5 A g^{-1} and good rate capability of 73.6% capacitance retention at 20 A g^{-1} in 6M KOH electrolyte. Furthermore, the assembled zinc ion capacitor still revealed outstanding capacitance of 335 F g^{-1} at 0.1 A g^{-1}, excellent cycling stability of 92.2% capacitance retention after 10 000 cycles and ultra-high energy density of 150.3 Wh kg^{-1} at power density of 90 W kg^{-1} in 3M $ZnSO_4$ electrolyte. It is believed that the current work provides a facile and effective strategy to recycle PET waste into high-valuable MOF, and further expands the applications of MOF-derived carbons for high-performance energy storage devices, so it is conducive to both pollution alleviation and sustainable economic development.

Keywords: PET; Recycling; Porous carbon; Supercapacitor; Energy storage

1. Introduction

Since the first synthesis of polyethylene terephthalate (PET) fibers in the mid-1940 s by DuPont chemists, PET have been widely used in textiles, packaging, carpeting, and single-use beverage bottles [1–4]. From global statistics, the overall

* Corresponding authors.Faculty of Chemical Technology and Engineering, West Pomeranian University of Technology, Piastów Ave. 42, 71-065, Szczecin, Poland
E-mail addresses: hgwenxin@126.com (X. Wen), ttang@ciac.ac.cn (T. Tang), xchen@zut.edu.pl (X. Chen).

https://doi.org/10.1016/j.gee.2023.01.002

consumption of PET amounts to 50–60 million tons a year and continues to increase [5,6]. After completed their service, most of these non-biodegradable PET products are directly thrown away as garbage, resulting in serious environment pollution and resource waste [7,8]. Therefore, it is highly desirable to develop environmentally friendly and cost-effective strategies for recycling PET wastes with the aim of resources preservation and environment protection.

To date, extensive investigations have been carried out for the recycling of PET wastes [9,10]. Similar to the recycling of ordinary polymer wastes, PET wastes can be treated by landfill and incineration, which have to face the problems of resources waste and the secondary pollution. Essentially, they are not promising strategies to meet the principles of circular economy with recyclability and sustainability. In contrast, chemical recycling is a relatively better approach to convert PET chain into its building units via a depolymerization process, in which some useful products are harvested, such as monomers, oils and chemicals [11,12]. Further, considering that main constituent of PET depolymerization is 1,4-benzendicarboxylic acid (BDC), which is the main organic linker of many crystalline porous structures, it is more promising to convert waste PET into metal organic frameworks (MOFs). Up to now, a series of MOFs, such as MIL-53(Cr, Al, Ga) [13], MIL-101(Cr) [14], MIL-47(V) [15], Ni-MOF [6], MOF 5 [16], Tb-BDC [17], UiO-66(Zr) [18] were successfully synthesized via a stepwise process, involving firstly the depolymerization of PET into BDC, and then combining the BDC with metal salts in the second step. For example, Rajagopal et al. [16] reported PET bottles as a linker source towards MOF synthesis, where PET was firstly depolymerized into BDC by a microwave-assisted alkaline procedure, then the purified BDC reacted with zinc acetate to form MOF 5. Similarly, Al-Enizi group [6] depolymerized waste PET bottles into BDC in a high-pressure reactor via hydrothermal reaction, then the BDC was coordinated with Ni^{2+} to produce Ni-MOF. Generally, the conversion of PET into BDC are required in harsh experimental conditions including high temperature, long reaction time and the presence of acids/bases catalysts. Notably, Deleu et al. [19] suggested a one-pot route to synthesize MIL-53(Al) and MIL-47(V) via the combining metal salts and PET wastes in a microwave oven. Recently Cho et al. [2] also reported the direct recycling of PET waste to fabricate MIL-53(Al)) via a one-pot hydrothermal reaction at 220 °C under self-generated pressure. Although some positive progresses have been made to achieve the simultaneous depolymerization of PET waste and the controllable synthesis of MOFs, there are still some challenges, such as unsatisfied conversion efficiency of PET, ununiform morphology of MOFs, tedious separation/purification steps, etc., which largely limit the large-scale production and potential applications of PET based MOFs.

Recently porous carbon materials have attracted ever-increasing attraction as electrode materials for supercapacitors, but it remains a great difficulty to control their pore structure with optimal electrochemical performances [20,21]. MOFs derived porous carbons are getting more attention due to their unique porosity, chemical stability, high specific surface area and good conductivity. Consequently, various types of MOFs have been extensively exploited as carbon precursors for the synthesis of supercapacitive electrodes [22,23]. Liu et al. [24] reported a MOF-5 derived nanoporous carbon for electrochemical double-layer capacitors, exhibiting the specific capacitance of 204 F g^{-1} at 5 mV s^{-1}, which was higher than that of the ordered mesoporous silica material SBA-15. Wang et al. [25] used ZIF-8 to derive porous carbon polyhedrons (PCPs) to prepare nanoporous carbon as the negative electrode of an aqueous-electrolyte based asymmetric supercapacitor, which demonstrated a high capacitance of 245 F g^{-1} at 1 A g^{-1} with a maximum energy density of 25.4 W h·kg^{-1} at 400 W kg^{-1} and retaining 93% capacitance after 10000 cycles. Guo et al. [26] reported a hierarchical porous Zr-MOF (HP-UiO-66), and the derived carbon as electrodes corresponded to a high specific capacitance of 849 F g^{-1} at 0.2 A g^{-1}. Yaghi et al. [27] investigated a series of carbons from M-MOF-74 as electrode materials for supercapacitors, and found that highly mixed metals in this MOF series displayed better performances because of the redox reactions during the charge/discharge process. Based on these pioneering studies, MOFs are a type of promising carbon precursors to produce high-quality porous carbon with excellent supercapacitor performances.

In the present study, direct recycling of waste PET bottles into MIL-53(Al) was proposed via a facile, economical and scalable hydrothermal process without catalysts, then the MOF-derived carbon was employed as electrodes for high-performance zinc-ion supercapacitors. As shown in Fig. 1, PET blocks and $Al(NO_3)_3$ reacted via a one-pot hydrothermal process with the DMF/H_2O mixture as solvent, resulting in 100% conversation of BDC into MIL-53(Al). After carbonization, the MOF-derived carbon exhibited high SSA of 1712 m^2 g^{-1}, large pore volume of 3.72 cm^3 g^{-1} and unique accordion-like structure with hierarchical porosity. Based on these advantageous characters, the obtained porous carbon was assembled into three-electrode supercapacitor and zinc ion capacitor, respectively. Interestingly, the assembled zinc ion capacitor displayed outstanding capacitance of 335 F g^{-1} at the current density of 0.1 A g^{-1}, excellent cycling stability of 92.2% capacitance retention after 10 000 cycles and ultra-high energy density of 150.3 Wh kg^{-1} at the power density of 90 W kg^{-1} in 3 M $ZnSO_4$ electrolyte. In brief, this work provides a facile and effective strategy to directly convert PET waste into MIL-53(Al), and the MOF-derived hierarchical porous carbons have great potentials in electrochemical energy storage applications.

2. Experimental

2.1. Materials

PET bottles were obtained from commercial soft drink packages in our city. $Al(NO_3)_3·9H_2O$, 4-benzendicarboxylic acid (BDC), $ZnSO_4$, dimethylformamide (DMF), acetone, KOH and multiwalled carbon nanotubes (CNT) were purchased from Sigma–Aldrich. Hydrochloric acid (HCl) was of analytical grade. All the chemical reagents were used as received without any further purification.

Please cite this article as: J. Li et al., Facile synthesis of accordion-like porous carbon from waste PET bottles-based MIL-53(Al) and its application for high-performance Zn-ion capacitor, Green Energy & Environment, https://doi.org/10.1016/j.gee.2023.01.002

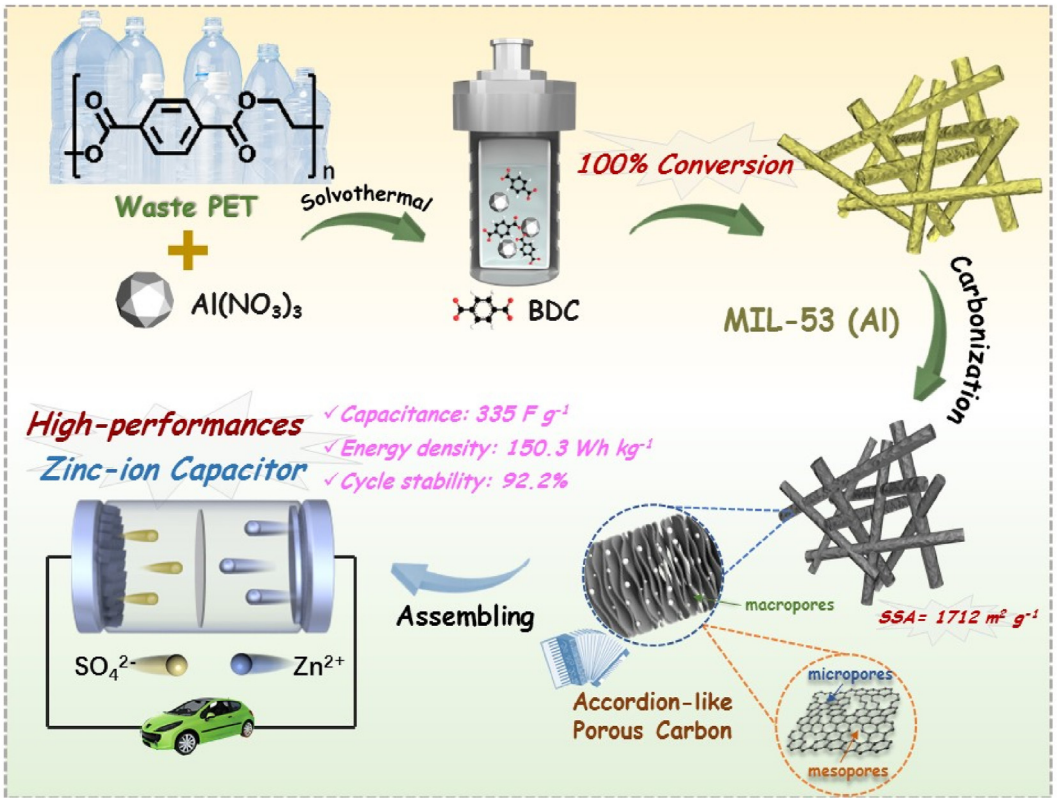

Fig. 1. Schematically illustration of direct recycling waste PET bottles into MIL-53(Al) and the derived porous carbon for high-performance Zinc-ion capacitor.

2.2. Synthetic procedures

2.2.1. Synthesis of MIL-53(Al) using waste PET bottle via a hydrothermal process

In a typical experiment, 5.0 g PET bottle slices (0.3 cm × 0.3 cm), 10.0 g $Al(NO_3)_3 \cdot 9H_2O$, 35 mL DMF and 15 mL deionized water were added into in a 100 mL Teflon-lined autoclave. The autoclave was sealed and heated at 180 °C for 12 h, then cooled to room temperature. The as-prepared product was washed with DMF and acetone for 3 times, respectively. After drying in vacuum at 80 °C for 24 h, the obtained white powder was 4.8 g (marked as PMD, the schematically growth process was shown in Fig. S1a). As a control, a similar experiment was carried out with 50 mL deionized water but without DMF at 180 °C for 12 h. This sample was labeled as PMH, which only harvested 2.37 g (the product morphologies of PMD and PMH was shown in Fig. S1b). Furthermore, the hydrothermal process with DMF/H_2O mixture as solvent was performed under different reaction time and marked as PMD-X (X = 3, 6 and 72 h). The conversation efficiency of PET was calculated based on the mass of BDC in MIL-53(Al). For PMD, it was 100 wt%; while for PMH, it was only 49.4 wt%.

2.2.2. Synthesis of MIL-53(Al) from BDC and $Al(NO_3)_3 \cdot 9H_2O$ via a hydrothermal process

Firstly 0.734 g $Al(NO_3)_3 \cdot 9H_2O$ was dissolved into 15 mL deionized water, while 0.770 g BDC was dissolved into 35 mL DMF. Subsequently these two solutions were mixed together with magnetic stirring for 30 min, then transferred into 100 mL Teflon-lined steel autoclave to heat at 180 °C for 24 h. The solid product was washed 3 times with DMF and acetone, respectively. After drying in a vacuum at 80 °C overnight, the resultant white powder was collected and its mass was 0.34 g (marked as PMD-P).

2.2.3. Carbonization of MIL-53(Al)

3.0 g of MIL-53(Al) was placed in a corundum boat and put into a tube furnace. After passing over Ar for 15 min, the furnace was heated to 800 °C at 6 °C min^{-1} and kept heating at this temperature for 3 h. After cooled to room temperature, the solid product was added into 5% HCl solution with magnetic stirring for 6 h. The product was washed 3 times by deionized water, then dried in a vacuum at 80 °C overnight (labeled as CPMD). As a control experiment, PET bottle slices (3.0 g) and PMH (3.0 g) were also treated at the same condition, and the restltant products were named as CP and CPMH, respectively. Furthermore, the CPMD were carbonized at 700 °C and at 900 °C respectively, which are labeled CPMD-700 and CPMD-900.

2.3. Materials characterization

Transmission electron microscopy (TEM) was performed on a FEI Tecnai F30 transmission electron microscope operating at an acceleration voltage of 200 kV. Scanning Electron Microscopy (SEM) and EDX mapping was done with a SEM, XL30ESEM-FEG with an acceleration voltage of 20 KV and

Please cite this article as: J. Li et al., Facile synthesis of accordion-like porous carbon from waste PET bottles-based MIL-53(Al) and its application for high-performance Zn-ion capacitor, Green Energy & Environment, https://doi.org/10.1016/j.gee.2023.01.002

energy-dispersive X-ray (EDX, OXFORD INSTRUMENTS X-MAX). X-ray diffraction (XRD) was recorded by a Philips diffractometer using Cu Kα radiation. The thermogravimetric analysis (TGA) was conducted on a DTA-Q600 SDT TA at a heating rate of 10 °C min^{-1} from room temperature to 900 °C under air atmosphere. The N_2 adsorption/desorption isotherms were carried out at 77 K using a Quantachrome Autosorb-1C-MS instrument, where Brunauer–Emmett–Teller (BET) and Density Functional Theory (DFT) methods were used to calculate the specific surface area and the pore size distribution. Raman scattering was measured with a Renishaw microRaman spectrometer (λ = 785 nm). The X-ray photoelectron spectra (XPS) were obtained using Al Kα (hν = 1486.6 eV) radiation with a Prevac system equipped with a Scienta SES 2002 electron energy analyzer operating at constant transmission energy (Ep = 50 eV).

2.4. Electrochemical measurements

The BioLogic Science Instruments (EC-LAB VMP3 multichannel generators) were used to evaluate the electrochemical performance. In a three-electrode system, carbon material (2.0 mg) was mixed with PTFE binding agent (0.2 mg) and carbon nanotubes (0.2 mg) in a mortar to achieve carbon suspension, then coated onto a nickel foam (1 × 1 cm^{2}). The working electrode was dried under vacuum at 70 °C for over 12 h and further pressed at 5 MPa for 6s. The counter electrode and reference electrode are a Pt plate and a Hg/HgO electrode, while the electrolyte is 6 M KOH.

For the Zn-ion capacitor, the slurry on grafoi was prepared with the same ratio of carbon materials, PTFE binder and carbon nanotubes. After drying in a vacuum at 60 °C overnight, the grafoil was cut into a disc with 10 mm in diameter with a mass loading of 2.54 mg cm^{-2}. According to the ratio of the active material, binder and conductive agents, the areal mass loading of the active material in the electrode was 2.03 mg cm^{-2}. The bare Zn metal foil (10 mm in diameter), the working electrode and glass fiber separator (GF/F, Whatman) were assembled in a Swagelok cell, where 3M $ZnSO_4$ solutions were employed as the electrolyte. The cyclic voltammetry (CV) and galvanostatic charge/discharge (GCD) were tested at the same voltage window from 0.005 V to 1.8 V and electrochemical impedance spectroscopy (EIS) measurements were carried out within the range of 100 kHz to 10 mHz. The gravimetric specific capacitance (C_{wt}, F g^{-1}), gravimetric energy (E_{wt}, Wh kg^{-1}) and gravimetric power densities (P_{wt}, W kg^{-1}) for a single electrode are calculated as:

$$C_{wt} = I\Delta t / m\Delta V$$

$$E_{wt} = C_{wt}\Delta V^2 / (2 * 3.6)$$

$$P_{wt} = E_{wt}/\Delta t$$

where I is the applied current (A), Δt is the discharge time (s), ΔV is the voltage window, and m is the total mass of the active material on the working electrode (g).

The volumetric capacity (C_{vol}, F cm^{-3}) of ZICs was calculated by the density of the active materials. The ρ (g cm^{-3}) was calculated by dividing the net mass of the electrode disk by its volume (V, cm^{-3}), and V was obtained by measuring the thickness (h, cm) of the electrode disk with sectional area (S, cm^2) of 0.785 cm^2 by using a micrometer.

$$V = S * h$$

$$\rho = m/V$$

$$C_{vol} = C_{wt} * \rho$$

The volumetric energy density (E_{vol}, Wh L^{-1}) of the cells were calculated as:

$$E_{vol} = E_{wt} * \rho$$

The volumetric power density (P_{vol}, W L^{-1}) of the cells were obtained as:

$$P_{vol} = P_{wt} * \rho$$

3. Results and discussions

3.1. Characterization of PET-derived MOFs and the MOFs-derived carbons

Fig. 2a schematically shows the crystal structure of MIL-53(Al), which is assembled via the coordination between Al^{3+} and the carbonyl groups of 1,4-benzendicarboxylic acid (BDC). To investigate the effect of solvent (with or without DMF) on the crystal structure of PET-derived MOFs, PMH and PMD were evaluated by XRD. As shown in Fig. 2b, both of them exhibited the characteristic diffraction peaks of MIL-53 (Al), but the peak intensities of PMD were relatively stronger than that of PMD, and some special peaks (at around 2θ = 13° and 23°) were detected in PMH curves, which should belong to the impurities [28,29]. Moreover, according to SEM and TEM images in Fig. 2c and d, PMD displayed a regular rod-like shape and well-crystallized fiber structure, while PMH was a mixture of short fibers and irregular plates (Fig. 2e and f). Besides, other rations of DMF/H_2O were also selected, but the impurity of MIL-53 (Al) was high or the conversation of PET was not complete. Therefore, we concluded that the mixture of DMF and H_2O with the best ratio of 35/15 played an important role to optimize the crystallized structure of MIL-53(Al), which is possibly ascribed to the better solubility to BDC for promoting the coordination with Al^{3+}.

In addition, the effect of reaction time (3 h–72 h) on morphology and yield of PET-derived MOFs was studied (Fig. S2). With the increase of reaction time from 3 h to 12 h, the shape gradually became regular. When the reaction time was prolonged into 72 h, it kept well-crystallized fiber structure. Meanwhile, the yield of PMD-72 was slightly higher than that of PMD-12. However, to achieve the balance on energy consumption and product yield, the reaction time was set for 12 h to synthesize PET-derived MIL-53(Al) in a large scale. In

Please cite this article as: J. Li et al., Facile synthesis of accordion-like porous carbon from waste PET bottles-based MIL-53(Al) and its application for high-performance Zn-ion capacitor, Green Energy & Environment, https://doi.org/10.1016/j.gee.2023.01.002

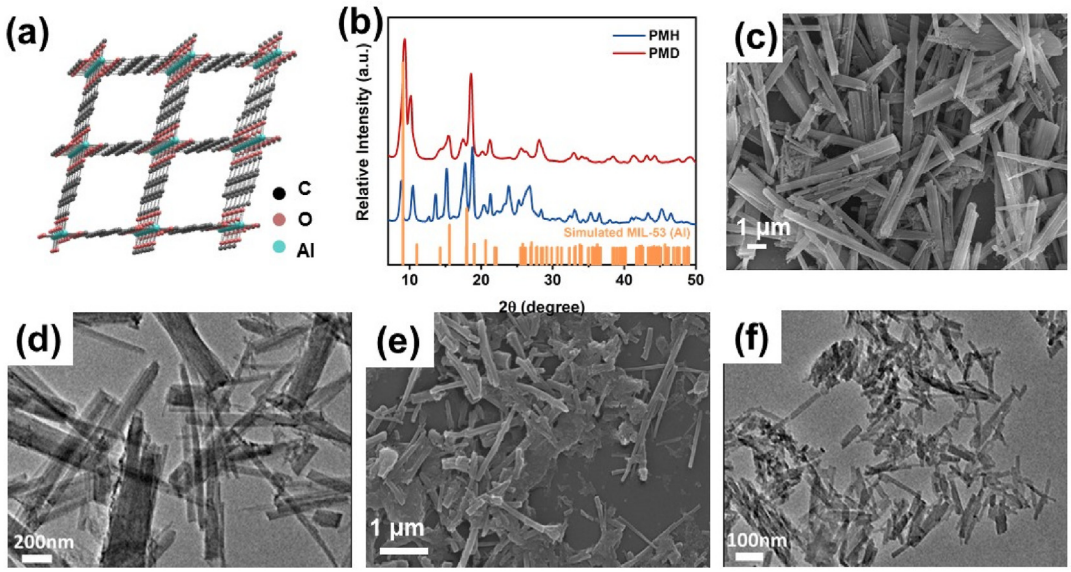

Fig. 2. (a) Schematic illustration of the structure of MIL-53(Al); (b) XRD patterns of PMH and PMD; (c) SEM and (d) TEM images of PMD; (e) SEM and (f) TEM images of PMH.

addition, PMD-P from BDC and $Al(NO_3)_3 \cdot 9H_2O$ via hydrothermal reaction was investigated. As shown in Fig. S3, it was composed of small and fairly uniform sized particles, and corresponded well to a typical diffraction peak of MIL-53 (Al). These results indicated that nanofibers like MIL-53 (Al) were only observed when PET was used as the source of BDC, which was ascribed to the restricted growth of MIL-53(Al). The depolymerization of PET and the growth of MIL-53(Al) occurred synchronously, so the BDC reacted in-situ with metal ions (Al^{3+}) on the unreacted PET surface with a certain direction, where the PET acted as a template and a structure-directing agent (Fig. S1a). In contrary, when BDC was used as the organic linker, the growth directions were unlimited, so the resultant MIL-53 (Al) were nanoparticles.

To synthesize porous carbons, the PET-derived MOFs were carbonized in nitrogen atmosphere. Fig. 3a shows their XRD curves (CPMD from PMD; CPMH from PMH). They exhibited two strong diffraction peaks at 24° and 43°, which were assigned to the characteristic peaks of (002) and (101) planes of graphitic carbon material [30,31]. According to the Raman spectra of CPMD and CPMH in Fig. 3b, the D-band at ~1314 cm^{-1} and the G-band at ~1606 cm^{-1} were visible [32]. We noted that the I_D/I_G ratio of CPMD (0.99) was lower than that of CPMH (1.32), suggesting that the CPMD has higher graphitization degree [33]. From SEM images in Fig. S4, the morphologies from CPMH and CPMD were similar, except for a slightly rougher surface from CPMD. Furthermore, Fig. 3c shows HRETM images of the CPMD. It was visible that there were a number of meso- and micropores, which are favorable to the access and diffusion of electrolytes in electrode [34,35]. More importantly, these porous nanosheets were assembled in the fibers with accordion-like structure, which can effectively prevent the agglomeration and overlap of nanosheets (Fig. 3c, inset), and promote the transmission of electrons and the movement of electrolytes [36,37]. In contrast, Fig. 3d shows the CPMH with a heterogeneous distribution of mesopores (some sheets are full of mesopores, but others are nonporous), which are unfavorable to the ion transport in electrolyte [35]. In addition, the thermal stability of CPMD and CPMH were analyzed by thermogravimetric analysis (TGA) at air atmosphere. It was found that the CPMD had lower thermal stability than the CPMH (Fig. S5). Generally the better crystalline structure and the higher graphitization degree of carbon materials, can result in better thermal stability [38,39]. Here the CPMD has lower thermal stability, which might be ascribed to its higher specific surface area (SSA) and higher content of oxygen. During heating, it was easier to occur thermal oxygen degradation with pore collapse and oxygen loss, leading to the rapid decrease on weight.

The surface element component of PET-derived carbons was characterized by X-ray photoelectron spectroscopy (XPS). As shown in Fig. 4a, they were mainly composed of carbon (C) and oxygen (O) elements. However, the oxygen content in CPMD was higher than that in CPMH (Fig. 4b). In Fig. 4c and d, the C1s spectrum of CPMD and CPMH was fitted into three peaks of C–C (284.6 eV), C═C (285.1 eV), C═O (286.3 eV) and O–C═O (288.7 eV) [31]. Similarly, as shown in Fig. 4e and f, the O1s spectrum was fit ed into two peaks at 531.2eV (C–O) and 533.2 eV (O–C═O). It was found that the relatively higher content of C═C in CPMD, which was ascribed to its higher graphitization degree. Meanwhile, the higher content of C═O in CPMD was present, implying more oxygen-containing functional groups on its surface, which is beneficial for increasing wettability between the electrolyte and carbon materials [40,41].

The porosity parameters of CPMD and CPMH were investigated by nitrogen adsorption/desorption measurements. As shown in Fig. 5a, they showed type IV isotherms, where a

Please cite this article as: J. Li et al., Facile synthesis of accordion-like porous carbon from waste PET bottles-based MIL-53(Al) and its application for high-performance Zn-ion capacitor, Green Energy & Environment, https://doi.org/10.1016/j.gee.2023.01.002

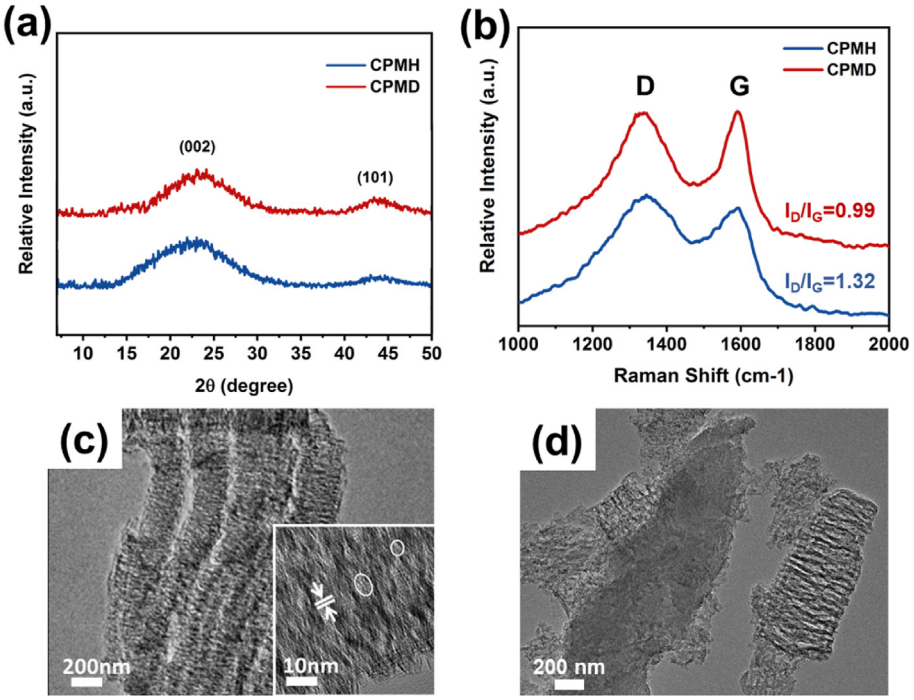

Fig. 3. (a) XRD curves and (b) Raman spectra of CPMH and CPMD; HRTEM images of (c) CPMD and (d) CPMH.

hysteresis loop at high relative pressure (P/P_0 = 0.4–0.9) can be clearly observed [42]. Generally the steep increase at a low relative pressure (P/P_0 < 0.02) represents the adsorption capacitance of micropores for N_2 (<2 nm) [43]. According to Brunauer–Emmett–Teller (BET) and Density Functional Theory (DFT) analysis, the detailed parameters are summarized in Table 1. The CPMD had a specific surface area (SSA) of 1712 $m^2\ g^{-1}$ and a total pore volume of 3.72 $cm^3\ g^{-1}$; while the values for CPMH were SSA = 1193 $m^2\ g^{-1}$ and V_{total} = 1.36 $cm^3\ g^{-1}$. As shown in Fig. 5b, the CPMH

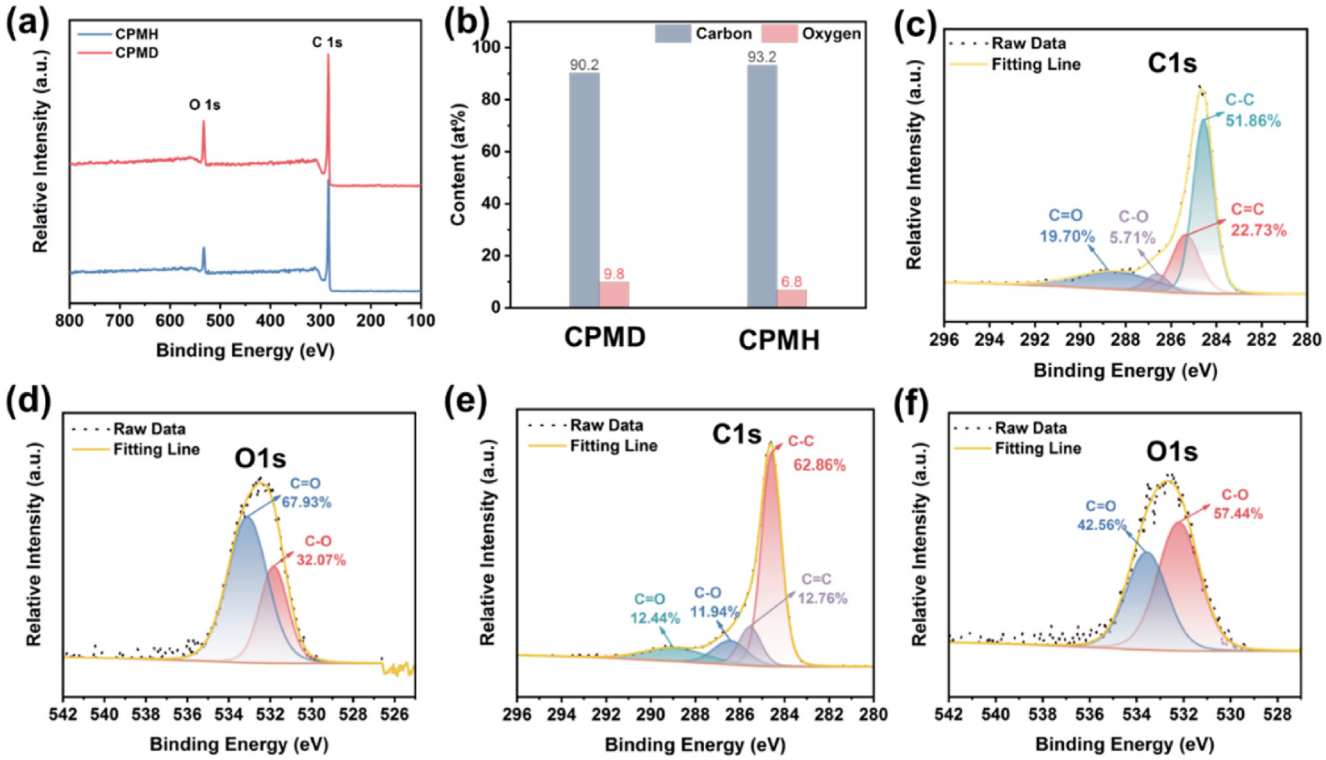

Fig. 4. (a) XPS survey spectra; (b) the atomic contents of CPMD and CPMH; high-resolution of (c, e) C1s and (d, f) O1s spectra of CPMD and CPMH.

Please cite this article as: J. Li et al., Facile synthesis of accordion-like porous carbon from waste PET bottles-based MIL-53(Al) and its application for high-performance Zn-ion capacitor, Green Energy & Environment, https://doi.org/10.1016/j.gee.2023.01.002

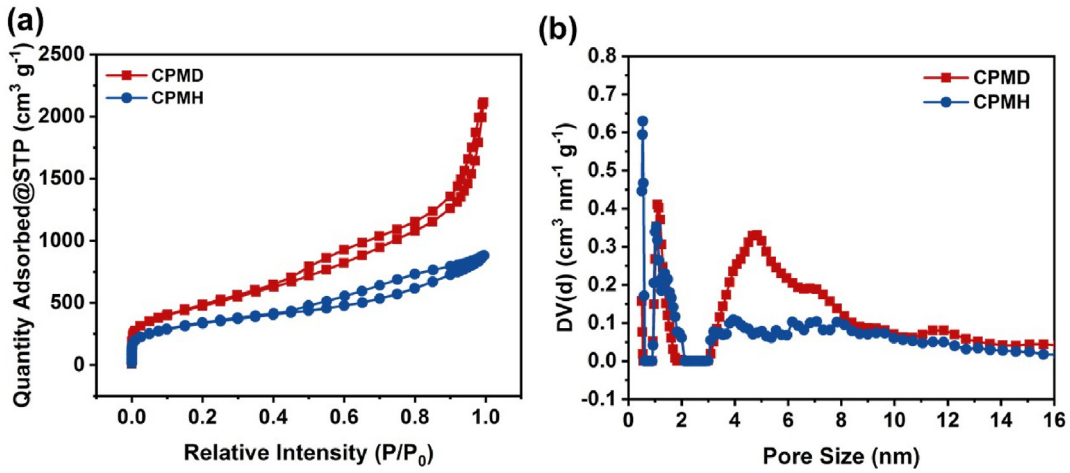

Fig. 5. (a) N_2-isotherms curves and (b) pore size distribution curves of CPMH and CPMD.

exhibited micropore size at 1.2 nm and mesopore size at 4.57 nm. In contrast, the mesopore size of CPMD was centered at 7.64 nm. Although both of them achieved hierarchical porous structure riddled with micropores, the percent value of $V_{meso(2\text{-}5nm)}/V_{total}$ in CPMH were higher than that in CPHD, which played important roles as the channels for electrolyte storage and transport throughout the porous structure [41,44]. Besides, the effect of carbonization temperature on porosity parameters was investigated. As shown in Fig. S6 and Table S1, CPMD-800 had the highest values for specific surface area (SSA) of 1712 $m^2\ g^{-1}$ and reasonable ratio of micropore/mesoporous, indicating that 800 °C was the optimal temperature to prepare carbons for supercapacitor electrodes.

3.2. Evaluation of electrochemical performances

The electrochemical properties of PET-MOF derived porous carbon were firstly evaluated in the three-electrode system with 6 M KOH as electrolyte. Here PET-derived carbon (denoted as CP) was also used as a comparison, which was amorphous structure with low graphitization degree (TEM image and Raman spectra are shown in Fig. S7). Fig. 6a shows the cyclic voltammetry (CV) curves of CP, CPMD and CPMH at a scan rate of 100 mV s^{-1}. All of them exhibited nearly rectangular shape without obvious redox peak, indicating an ideal capacitive behavior [45,46]. However, the largest CV loop area of CPMD represented the highest specific capacitance. Galvanostatic charge/discharge (GCD) curves at 0.5 A g for three samples are plotted in Fig. 6b. Each of them showed a quasi-triangle shape, implying the formation of an efficient electric double layer and fast ion transport in the carbon electrode [47]. In Fig. 6c, a specific capacitance of 391 F g^{-1} at 0.5 A g^{-1} was obtained for CPMD, which is higher than the CPMH (307 F g^{-1}) and the CP (39 F g^{-1}). Notably, the specific capacitance of CPMD was also much higher than most of previously reported MOF-derived carbon materials (Table S2). Meanwhile, the CPMD displayed the rate capacity of 288 F g^{-1} with a 73.6% capacitance retention at the current density of 20 A g^{-1} (Fig. 6c), which were better than other two samples (The data were calculated according to the GCD curves in Fig. S8).

Electrochemical impedance spectroscopy (EIS) is useful to investigate the process of ion transport/charge transfer within the carbon electrode [48,49]. The Nyquist plot shows a straight line and a semicircle in the high-frequency region. In Fig. 6d, the CPMD showed a nearly perpendicular straight line in the low-frequency region, suggesting the low equivalent series resistance (ESR). Furthermore, it had the smallest radius with a charge transfer resistance (R_{ct}) of 0.72 Ω (Fig. 6e). In addition, the Bode plots show the relationship between phase angle and frequency (Fig. 6f). The phase angle of CPMD was −83° at 0.01 Hz, indicating a fast frequency response [50]. The characteristic frequency (f_0) for a phase angle of −45° was 1.23 Hz for the CPMD, so the corresponding time constant τ_0 ($\tau_0 = 1/f_0$) was 0.81 s, which was lower than that of the CPMH (1.04 s) and the CP (7.8 s). These results conjointly indicated

Table 1
Porosity properties of CPMH and CPMD samples.

Samples	S_{BET} [a] ($m^2\ g^{-1}$)	V_{total} [b] ($cm^3\ g^{-1}$)	V_{micro}/V_{total} (%)	$V_{meso(2\text{-}5nm)}/V_{total}$(%)	Average Pore Size (nm)
CPMH	1193	1.36	62.0	12.7	4.57
CPMD	1712	3.72	30.0	24.0	7.64

[a] specific surface area was calculated by BET method at $p/p_0 = 0.003–0.1$.
[b] total pore volume at $p/p_0 = 0.99$.

Please cite this article as: J. Li et al., Facile synthesis of accordion-like porous carbon from waste PET bottles-based MIL-53(Al) and its application for high-performance Zn-ion capacitor, Green Energy & Environment, https://doi.org/10.1016/j.gee.2023.01.002

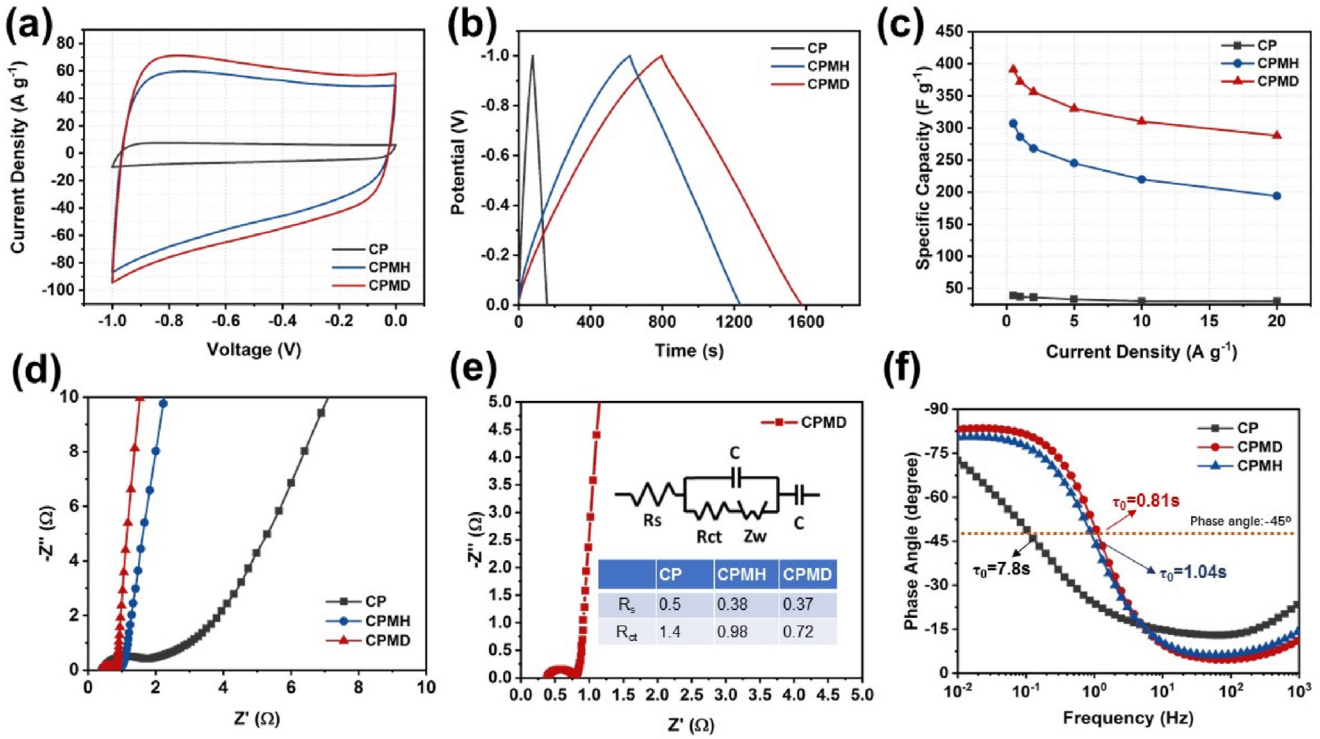

Fig. 6. Electrochemical performances of PET-derived carbon samples in three-electrode 6 M KOH cell: (a) CV curves at 100 mV s^{-1}; (b) GCD curves at 0.5 A g^{-1}; (c) rate performance from 0.5 to 20 A g^{-1}; (d) Nyquist plots of CP, CPMH and CPMD; (e) impedance data of CPMD (inset: equivalent circuit and fitted resistances); (f) Bode plots for CP, CPMH, and CPMD.

better ion transport behavior from the CPMD due to its rational hierarchical porosity and larger ion-accessible surface area.

As typical two-electrode asymmetric supercapacitor, Zn-ion capacitor (ZIC) has been expected as energy storage for practical application [51]. The CPMD as cathode and Zn foil as anode using 3M $ZnSO_4$ as the electrolyte were assembled into ZIC (Fig. 7a). As shown in Fig. 7b, nearly symmetrical equicrural triangles for GCD curves suggested a combination of battery and supercapacitor storage mechanisms [46,52]. Meanwhile, the CPMD had a capacitance of 335 F g^{-1} at the current density of 0.1 A g^{-1} (the corresponded volumetric capacitance was 57 F cm^{-3}, which was tested and calculated in Fig. S9, Tables S3 and S4). With the increase of the current density from 0.2 to 20 A g^{-1}, the corresponded specific capacitance gradually decreased from 295 to 144 F g^{-1} (Fig. 7c). When the current density was returned to 0.1 A g^{-1}, the specific capacitance of was 326 F g^{-1}, suggesting 97.3% of the initial capacitance was retained. Fig. 7d presents the cycling stability of ZIC. After 10 000 cycles, highly reversible and similar GCD curves were present, and the specific capacitance was 92.2% of the initial value. This suggests good structural stability and a fast kinetics response for ZIC [53,54]. In Fig. 7e, the energy density of the CPMD based ZIC reached to 150.3 Wh kg^{-1} at the power density of 90 W kg^{-1}, which is comparable to most LIBs and other reported ZICs. Besides, the capacity retention was compared with other ZICs, which is also higher than reported values [44,52,56–58,60]. Moreover, other PMD-derived samples at different carbonization temperature were also assembled into ZICs, and their electrochemical data are shown in Fig. S10). The results indicated the optimal carbonization temperature was 800 °C, where the obtained carbon corresponded to the best electrochemical performances in ZIC device.

The contributions from EDLC and pseudocapacitance can be evaluated as follows [56,58,59]:

$$i(V) = av^b \tag{1}$$

$$\log i(V) = \log a + b \log v \tag{2}$$

where a and b are constants that are fit, v is the scan rate (mV s^{-1}) and i is the peak current (mA). When $b = 1$, the current is dominated by the surface capacitance; whereas $b = 0.5$, there is a diffusion-controlled process [64]. Fig. 8a plotted the CV curves of the CPMD sample at different scan rates. In Fig. 8b, the value of b was 0.80 ($0.5 < 0.80 < 1$) at the scan rate of 1 mV s^{-1}, suggesting a "cooperative effect" between diffusion-controlled and surface-controlled processes [52].

The capacitive contribution was further calculated by the following Equion [46]:

$$i(V) = k_1 v + k_2 v^{1/2} \tag{3}$$

where k_1 and k_2 are constants, and $k_1 v$ and $k_2 v^{1/2}$ refer to surface- and diffusion-controlled processes respectively [41]. Fig. 8c compared the capacitive and diffusion contribution at 1 mV s^{-1}. It is clear that the diffusion was dominant because of its larger enclosed area. In Fig. 8d, the detailed percentages from capacitive and diffusion contribution are present. With

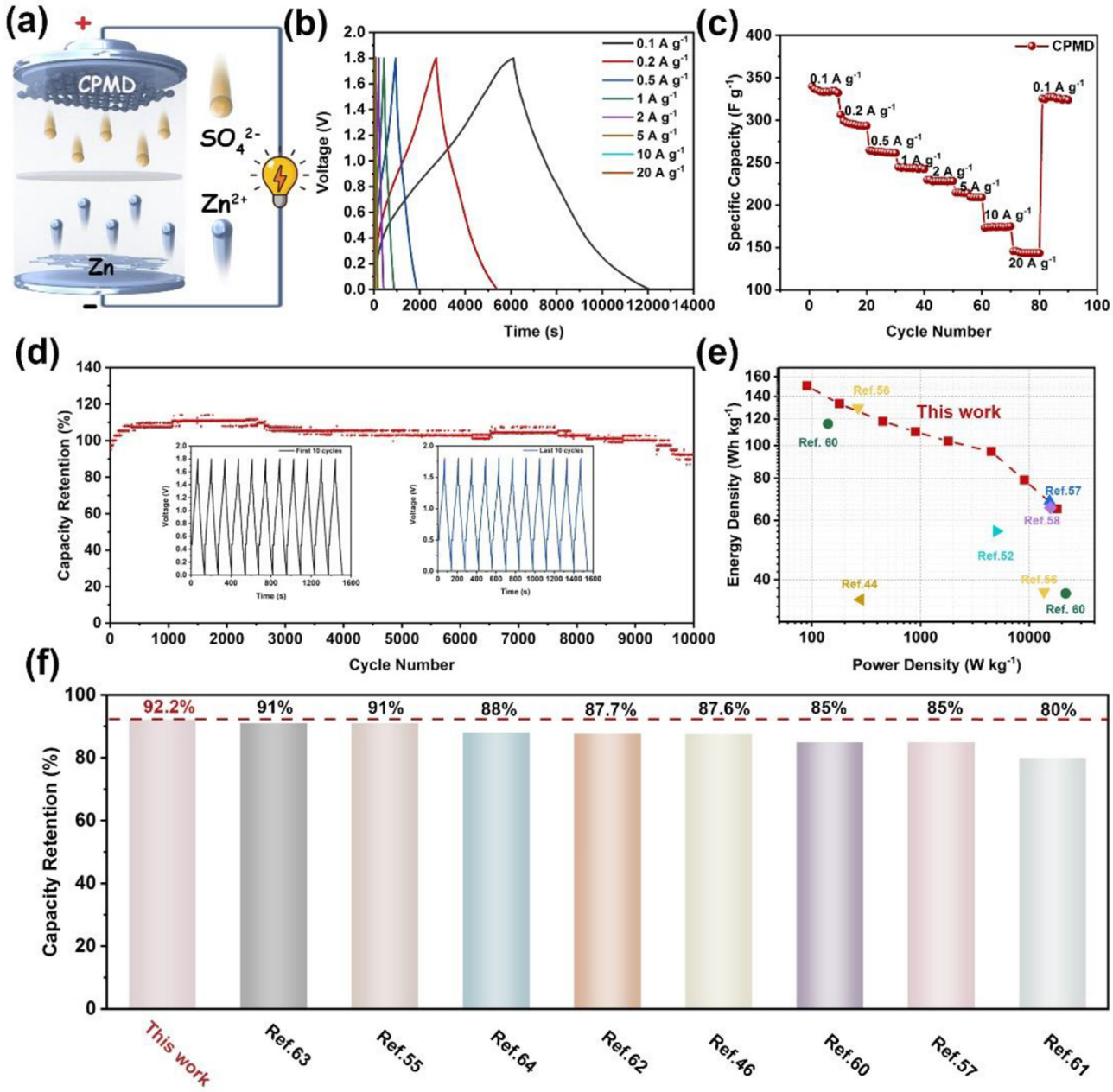

Fig. 7. Electrochemical data of CPMD in ZICs with 3M $ZnSO_4$ electrolyte: (a) Schematic illustration of a ZIC device; (b) GCD curves; (c) Rate performance; (d) Cycling stability of CPMD (Inset: GCD curves of the *first* and the *last* ten cycles from a long-term stability test). (e) Ragone plot (power density *vs* energy density) and (f) Long term cycle stability of CPMD versus reported results [46,55,57,60–64].

the increase of scan rate, the percentages for capacitive gradually increased; meanwhile the diffusion contribution showed a downward trend [40]. These results suggest that diffusion has larger contribution for the whole capacity at lower scan rates. However, when the capacitive type electrode has sufficient time to adsorb charges between the electrode and the electrolyte interface, more capacitive storage will be provided at the higher scan rates. Thus, it is demonstrated that our CPMD based ZIC device from MOF-derived porous carbon is the combination of both supercapacitor and battery.

Further, the ex-situ XRD was employed to analyze the energy storage mechanism of CPMD in ZICs system. In Fig. 9a shows the charge–discharge profiles under different states: the ZICs were firstly charged to 1.8 V from the open circuit voltage (at around 1.3 V), then discharge to 1.0 V and 0.2 V, and finally recharged to 1.0 V and 1.8 V. During the charge/discharge procedure, the surfaces of Zn foil gradually became rough, but zinc dendrite was undetectable (Fig. S11). As illustrated in Fig. 9b, the XRD patterns were very similar to each other during the charge/discharge stages, suggesting a

Please cite this article as: J. Li et al., Facile synthesis of accordion-like porous carbon from waste PET bottles-based MIL-53(Al) and its application for high-performance Zn-ion capacitor, Green Energy & Environment, https://doi.org/10.1016/j.gee.2023.01.002

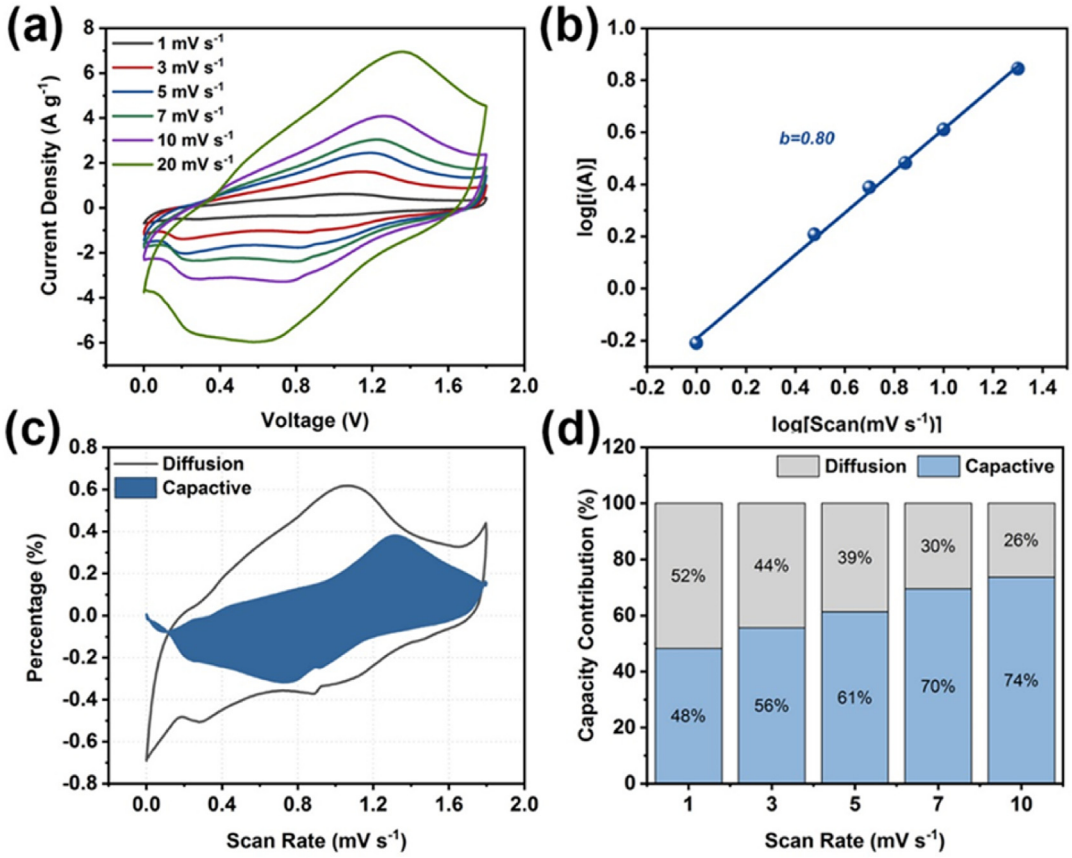

Fig. 8. (a) CV curves obtained at a scan rate from 1 mV s^{-1} to 20 mV s^{-1}; (b) Log(i) *vs* Log(v) and the line fit to the data along with the correlation factor *b*; (c) the capacitive contribution shown in the CV curve at 1 mV s^{-1}; (d) the percentage of the two contributions at different scan rates of the CPMD-based ZIC.

highly reversible stripping-depositing procedure. Meanwhile, the CPMD cathode was also recorded by ex-situ XRD. In Fig. 9c, the peaks located at 2θ = 18° and 28° were assigned to the PTFE, and the sharp peak at 26.4° belonged to the added CNTs as conductive agent, while others were corresponded to the diffraction peaks of the $Zn_4SO_4(OH)_6{\cdot}4H_2O$ (JCPDS: 44–0673) [65]. During the discharge procedures (from A to C), their intensity became stronger. When discharged to 0.2 V, they gradually disappeared (from D to E). These indicated the reversible generation and disappearance of $Zn_4SO_4(OH)_6{\cdot}4H_2O$. Based on above results, the charge/discharge storage process of ZICs could be described as follows [66,67]:

At the cathode:

(1) Physical adsorption/desorption

$$C//SO_4^{2-} + 2e^- = C + SO_4^{2-}$$

$$C + Zn^{2+} + 2e^- = C//Zn$$

(2) Chemical adsorption/desorption

$$C\cdots C{=}O + Zn^{2+}/H^+ + e^- = C\cdots C\cdots O\cdots Zn/C\cdots C\cdots O\cdots H$$

(3) Precipitation/dissolution

$$4Zn^{2+} + 6OH^- + SO_4^{2-} + 4H_2O = Zn_4SO_4(OH)_6{\cdot}4H_2O.$$

At the anode:

(4) $Zn = Zn^{2+} + 2e^-$

During the charge/discharge process, the adsorption and desorption of SO_4^{2-}, H^+, and Zn^{2+} were involved, which are highly dependent on the morphology and structure of cathode electrode. Considering the advantageous characters of CPMD as cathode electrode, the possible enhancement mechanism on electrochemical performance is illustrated in Fig. 9d: (i) the interconnected 3D structure from the stacked nanofibers is favorable to the transmission of electrolyte-ions;(ii) the unique accordion-like multilayer structure with high specific surface area enlarges the contact area between the electrode and electrolyte; (iii) the relatively high oxygen content enhances the wettability and decreases the resistance of the electrode/electrolyte interface; (iv) the hierarchical structure (the rational combination of macro-, meso- and micro-pores) facilitates rapid transport with short diffusion distances. In brief, the synergistic effect of these advantages resulted in excellent capacitive behavior of CPMD.

To verify the feasibility of ZIC for energy storage, the CPMD-derived single ZIC device was used to continuously

Please cite this article as: J. Li et al., Facile synthesis of accordion-like porous carbon from waste PET bottles-based MIL-53(Al) and its application for high-performance Zn-ion capacitor, Green Energy & Environment, https://doi.org/10.1016/j.gee.2023.01.002

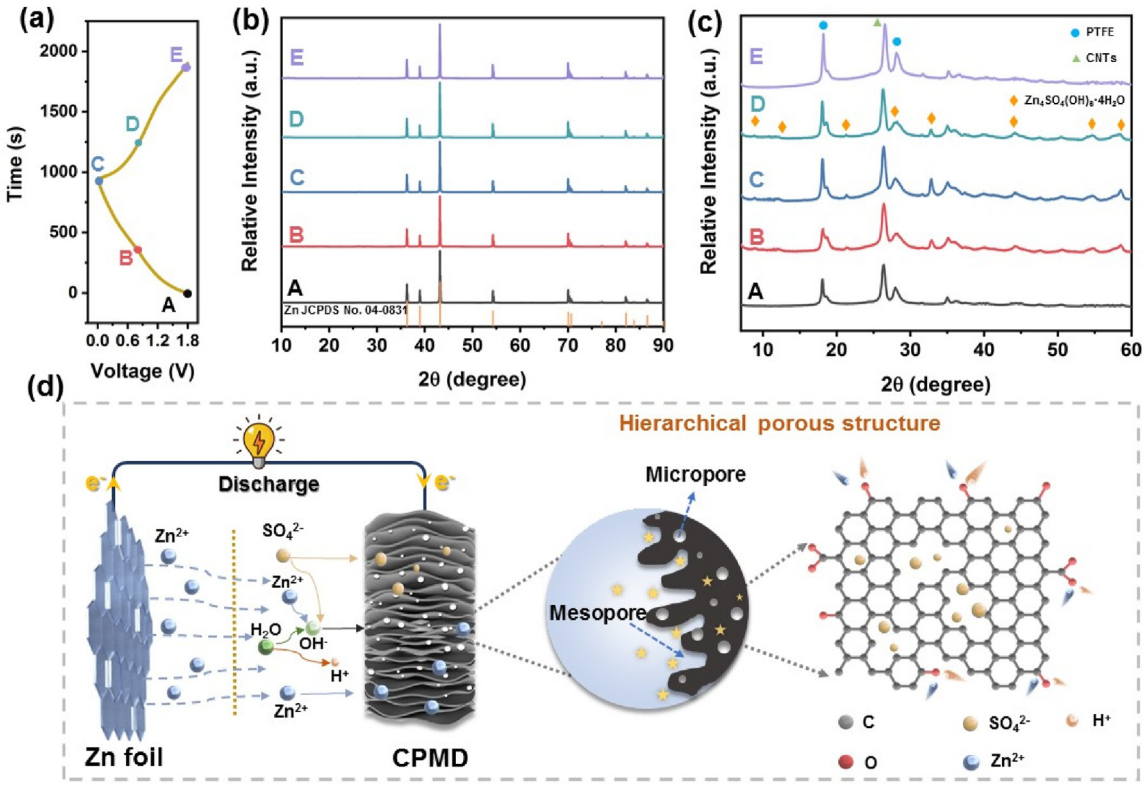

Fig. 9. Storage mechanism of CPMD based ZICs: (a) charge–discharge profiles under different states (A: charged to 1.8 V from OCV; B, C: discharged to 1.0 V and 0.2 V; D, E: charged to 1.0 V and 1.8 V); Ex-situ XRD profiles of (b) Zn foil and (c) CPMD electrode under different charge/discharge states; (d) Schematic mechanism of the MIL-53 (Al)-based porous carbon in ZICs.

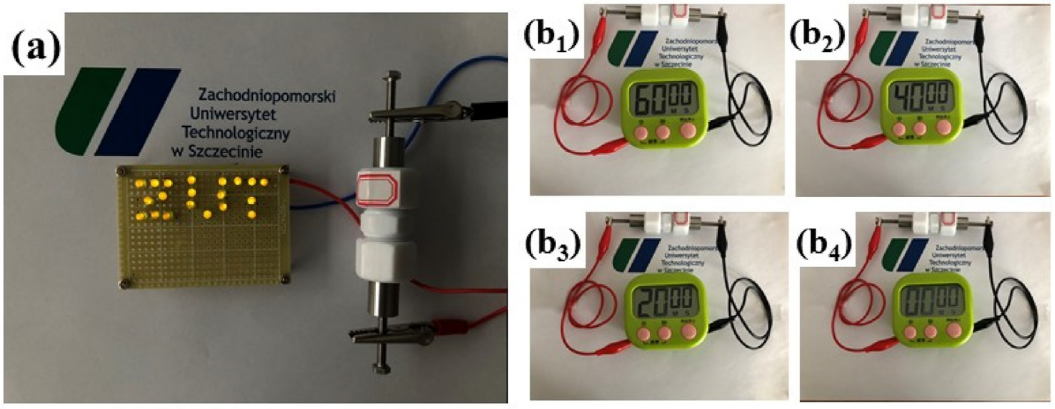

Fig. 10. The digital photos of (a) 20 yellow LEDs and (b_1-b_2) timer from 60 min with almost the same brightness by a MIL-53 (Al)-based porous carbon ZIC. (configured in a Swagelock cell).

power LEDs. As shown in Fig. 10a, 20 yellow LEDs were lighted up and lasted approximately 91 s. Furthermore, the CPMD-derived ZIC device was employed as the power supply of a timer (Fig. 10b). It was found that the ZIC can uninterruptedly power the timer as long as 60 min, and the brightness was almost the same as the beginning. These results vividly demontaded the feasibility of the porous carbon from waste PET derived MOF as ZIC electrodes for energy storage and output.

4. Conclusions

A directly recycle waste PET bottles into MIL-53(Al) was developed via a hydrothermal process, and subsequently the MOF-derived porous carbon was used as high-performance Zn-ion capacitor. The as-prepared carbon possessed unique accordion-like structure, high SSA and hierarchical porous distribution. These physicochemical features could enhance interfacial active sites, rapid ion-diffusion channels, and short

Please cite this article as: J. Li et al., Facile synthesis of accordion-like porous carbon from waste PET bottles-based MIL-53(Al) and its application for high-performance Zn-ion capacitor, Green Energy & Environment, https://doi.org/10.1016/j.gee.2023.01.002

ion transport distance, resulting in excellent electrochemical performance. We believe this work will not only provides a facial and cost-effective strategy to recycle waste PET bottles, but also proposes its application as high-performance supercapacitors. In the next step, waste PET bottles can be expanded to other PET products (such as PET membranes, PET fabrics, etc.); meanwhile the Al^{3+} can be replaced by other metal ions (such as Fe^{3+}, Zn^{2+}, Co^{2+}, Ni^{2+}, etc.). In summary, we want to fabricate various PET-derived MOFs and develop their applications in the field of green energy storage.

Author statement

Jiaxin Li: Investigation, Data curation, Writing- Original draft. **Shuai Zhang**: Investigation, Data curation. **Yumeng Hua:** Investigation, Data curation. **Yichao Lin:** Investigation, Formal analysis. **Xin Wen**: Formal analysis, Writing-Review & Editing, Supervision. **Ewa Mijowska**: Supervision, Writing -Review & Editing. **Tao Tang**: Supervision, Writing-Review & Editing. **Xuecheng Chen:** Supervision, Writing-Review & Editing, Project administration. **Rodney S. Ruoff**: Supervision, Writing-Review & Editing.

Declaration of competing interest

The authors declare that they have no known competing financial interests or personal relationships that could have appeared to influence the work reported in this paper.

Acknowledgments

The authors are grateful for the financial support from the NCN, Poland, UMO-2020/39/B/ST8/02937 and NAWA, 2020 PPN/BEK/2020/1/00129/ZAS/00001, and RSR appreciates support from the Institute for Basic Science (IBS-R019-D1).

Appendix A. Supplementary data

Supplementary data to this article can be found online at https://doi.org/10.1016/j.gee.2023.01.002.

References

[1] A.F. Sousa, R. Patrício, Z. Terzopoulou, D.N. Bikiaris, T. Stern, J. Wenger, K. Loos, N. Lotti, V. Siracusa, A. Szymczyk, S. Paszkiewicz, K.S. Triantafyllidis, A. Zamboulis, M.S. Nikolic, P. Spasojevic, S. Thiyagarajan, D.S. Van Es, N. Guigo, Green Chem. 23 (2021) 8795–8820.
[2] E. Cho, S.Y. Lee, J.W. Choi, S.H. Kim, K.W. Jung, Separ. Purif. Technol. 279 (2021), 119719.
[3] C. Song, B. Zhang, L. Hao, J. Min, N. Liu, R. Niu, J. Gong, T. Tang, Green Energy Environ 7 (2022) 411–422.
[4] F. Li, X. Dai, W. Qi, Green Energy Environ. 5 (2020) 453–460.
[5] M. Volanti, D. Cespi, F. Passarini, E. Neri, F. Cavani, P. Mizsey, D. Fozer, Green Chem. 21 (2019) 885–896.
[6] A.M. Al-Enizi, M. Ubaidullah, J. Ahmed, T. Ahamad, T. Ahmad, S.F. Shaikh, M. Naushad, Compos. B Eng. 183 (2020), 107655.
[7] A.K. Singh, R. Bedi, B.S. Kaith, Compos. B Eng. 219 (2021), 108928.
[8] M. Asensio, P. Esfandiari, K. Nunez, J.F. Silva, A. Marques, J.C. Merino, J.M. Pastor, Compos. B Eng. 200 (2020), 108365.
[9] P. Benyathiar, P. Kumar, G. Carpenter, J. Brace, D.K. Mishra, Polymers 14 (2022) 2366.
[10] N.a.S. Suhaimi, F. Muhamad, N.A. Abd Razak, E. Zeimaran, Polym. Eng. Sci. 62 (2022) 2355–2375.
[11] J. Chu, Y. Cai, C. Li, X. Wang, Q. Liu, M. He, Waste Manag. 124 (2021) 273–282.
[12] M.D.D. Caputto, R. Navarro, J.L. Valentin, A. Marcos-Fernandez, J. Polym. Sci. (2022) 1–15.
[13] S.H. Lo, D.S. Raja, C.W. Chen, Y.H. Kang, J.J. Chen, C.H. Lin, Dalton Trans. 45 (2016) 9565–9573.
[14] T.K. Vo, J.H. Kim, H.T. Kwon, J. Kim, J. Ind. Eng. Chem. 80 (2019) 345–351.
[15] T. Yoshioka, T. Motoki, A. Okuwaki, Ind. Eng. Chem. Res. 40 (2001) 75–79.
[16] P.K. Roy, A. Ramanan, C. Rajagopal Manju, Mater. Lett. 106 (2013) 390–392.
[17] F. Zhang, S.Y. Chen, S.Q. Nie, J. Luo, S.M. Lin, Y. Wang, H. Yang, Polymers 11 (2019) 1529.
[18] X. Dyosiba, J.W. Ren, N.M. Musyoka, H.W. Langmi, M. Mathe, M.S. Onyango, Ind. Eng. Chem. Res. 58 (2019) 17010–17016.
[19] W.P.R. Deleu, I. Stassen, D. Jonckheere, R. Ameloot, D.E. De Vos, J. Mater. Chem. A 4 (2016) 9519–9525.
[20] Y.L. Wen, X.G. Liu, X. Wen, X.C. Chen, K. Szymanska, R. Dobrzynska, E. Mijowska, Compos. B Eng. 199 (2020), 108256.
[21] Y.X. Zhang, L. Sun, L.K. Zhang, X.W. Li, J.L. Gu, H.C. Si, L. Wu, Y. Shi, C. Sun, Y.H. Zhang, Compos. B Eng. 182 (2020), 107611.
[22] L. Sun, Y.Y. Cai, M.K. Haider, D. Miyagi, C.H. Zhu, I.S. Kim, Compos. B Eng. 236 (2022), 109812.
[23] C.W. Ye, L. Xu, Compos. B Eng. 225 (2021), 109256.
[24] B. Liu, H. Shioyama, T. Akita, Q. Xu, J. Am. Chem. Soc. 130 (2008) 5390–5391.
[25] H. Yi, H. Wang, Y. Jing, T. Peng, X. Wang, J. Power Sources 285 (2015) 281–290.
[26] W. Gao, D. Chen, H. Quan, R. Zou, W. Wang, X. Luo, L. Guo, ACS Sustain. Chem. Eng. 5 (2017) 4144–4153.
[27] K.M. Choi, H.M. Jeong, J.H. Park, Y.-B. Zhang, J.K. Kang, O.M. Yaghi, ACS Nano 8 (2014) 7451–7457.
[28] D. Paszun, T. Spychaj, Ind. Eng. Chem. Res. 36 (1997) 1373–1383.
[29] F. Liu, J. Cao, Z. Yang, W. Xiong, Z. Xu, P. Song, M. Jia, S. Sun, Y. Zhang, X. Zhong, J. Colloid Interface Sci. 581 (2021) 195–204.
[30] J.X. Li, B. Michalkiewicz, J.K. Min, C.D. Ma, X.C. Chen, J. Gong, E. Mijowska, T. Tang, Chem. Eng. J. 360 (2019) 250–259.
[31] X. Liu, Y. Wen, X. Chen, A. Dymerska, R. Wróbel, J. Zhu, X. Wen, Z. Liu, E. Mijowska, ACS Appl. Energy Mater. 3 (2020) 8562–8572.
[32] X. Liu, C. Ma, J. Li, B. Zielinska, R.J. Kalenczuk, X. Chen, P.K. Chu, T. Tang, E. Mijowska, J. Power Sources 412 (2019) 1–9.
[33] X. Liu, C. Ma, Y. Wen, X. Chen, X. Zhao, T. Tang, R. Holze, E. Mijowska, Carbon 171 (2021) 819–828.
[34] Y. Zhou, Q. Huang, C.T.J. Low, R.I. Walton, T. Mcnally, C. Wan, New J. Chem. 43 (2019) 5632–5641.
[35] Y. Xi, J. Cao, J. Li, P. Zhang, Y. Zhu, W. Han, J. Energy Storage 37 (2021), 102470.
[36] C. Cheng, S. He, C. Zhang, C. Du, W. Chen, Electrochim. Acta 290 (2018) 98–108.
[37] Y. Li, S. Liu, Y. Liang, Y. Xiao, H. Dong, M. Zheng, H. Hu, Y. Liu, ACS Sustain. Chem. Eng. 7 (2019) 13827–13835.
[38] Z. Xing, L. Zhang, G. Pang, J. Xu, X. Wang, C. Yang, Diam. Relat. Mater. 120 (2021) 13287–13835.
[39] J. Li, X. Chen, J. Gong, J. Zhu, E. Mijowska, Diam. Relat. Mater. 105 (2020), 107802.
[40] W. Du, J. Xiao, H. Geng, Y. Yang, Y. Zhang, E.H. Ang, M. Ye, C.C. Li, J. Power Sources 450 (2020), 227716.
[41] J. Yin, W. Zhang, W. Wang, N.A. Alhebshi, N. Salah, H.N. Alshareef, Adv. Energy Mater. 10 (2020), 2001705.
[42] L. Yan, T. Liu, X. Zeng, L. Sun, X. Meng, M. Ling, M. Fan, T. Ma, Carbon 187 (2022) 145–152.

Please cite this article as: J. Li et al., Facile synthesis of accordion-like porous carbon from waste PET bottles-based MIL-53(Al) and its application for high-performance Zn-ion capacitor, Green Energy & Environment, https://doi.org/10.1016/j.gee.2023.01.002

[43] L. Wang, C. Yang, S. Dou, S. Wang, J. Zhang, X. Gao, J. Ma, Y. Yu, Electrochim. Acta 219 (2016) 592–603.
[44] Z. Pan, Z. Lu, L. Xu, D. Wang, Appl. Surf. Sci. 510 (2020), 145384.
[45] S. Umezawa, T. Douura, K. Yoshikawa, Y. Takashima, M. Yoneda, K. Gotoh, V. Stolojan, S.R.P. Silva, Y. Hayashi, D. Tanaka, Carbon 184 (2021) 418–425.
[46] Y. Zheng, W. Zhao, D. Jia, Y. Liu, L. Cui, D. Wei, R. Zheng, J. Liu, Chem. Eng. J. 387 (2020), 124161.
[47] P. Mehra, C. Singh, I. Cherian, A. Giri, A. Paul, ACS Appl. Energy Mater. 4 (2021) 4416–4427.
[48] H.T. Sun, L. Mei, J.F. Liang, Z.P. Zhao, C. Lee, H.L. Fei, M.N. Ding, J. Lau, M.F. Li, C. Wang, X. Xu, G.L. Hao, B. Papandrea, I. Shakir, B. Dunn, Y. Huang, X.F. Duan, Science 356 (2017) 599–604.
[49] Z. Li, D. Chen, Y. An, C. Chen, L. Wu, Z. Chen, Y. Sun, X. Zhang, Energy Storage Mater. 28 (2020) 307–314.
[50] Y.Q. Wang, B. Fugetsu, Z.P. Wang, W. Gong, I. Sakata, S. Morimoto, Y. Hashimoto, M. Endo, M. Dresselhaus, M. Terrones, Sci. Rep.-UK 7 (2017), 40259.
[51] F. Zhang, C. Wang, J. Pan, F. Tian, S. Zeng, J. Yang, Y. Qian, Mater. Today Energy 17 (2020), 100443.
[52] J. Li, J. Zhang, L. Yu, J. Gao, X. He, H. Liu, Y. Guo, G. Zhang, Energy Storage Mater. 42 (2021) 705–714.
[53] P. Liu, W. Liu, Y. Huang, P. Li, J. Yan, K. Liu, Energy Storage Mater. 25 (2020) 858–865.
[54] P. Yu, Y. Zeng, Y. Zeng, H. Dong, H. Hu, Y. Liu, M. Zheng, Y. Xiao, X. Lu, Y. Liang, Electrochim. Acta 327 (2019), 134999.
[55] Q. Wang, S. Wang, X. Guo, L. Ruan, N. Wei, Y. Ma, J. Li, M. Wang, W. Li, W. Zeng, Adv. Electron. Mater. 5 (2019), 1900537.
[56] S. Liu, X. Chen, Q. Zhang, J. Zhou, Z. Cai, A. Pan, ACS Appl. Mater. Interfaces 11 (2019) 36676–36684.
[57] H. Wang, M. Wang, Y. Tang, Energy Storage Mater. 13 (2018) 1–7.
[58] M.Z. Iqbal, M.M. Faisal, M. Sulman, S.R. Ali, A.M. Afzal, M.A. Kamran, T. Alharbi, J. Energy Storage 29 (2020), 101324.
[59] Y. Lu, Z. Li, Z. Bai, H. Mi, C. Ji, H. Pang, C. Yu, J. Qiu, Nano Energy 66 (2019), 104132.
[60] J. Zhang, S. Wei, H. Wang, H. Liu, Y. Zhang, S. Liu, Z. Wang, X. Lu, ChemSusChem 14 (2021) 2076–2083.
[61] X. Fan, X. Wen, Y. Tang, W. Zhou, K. Xiang, H. Chen, Electrochim. Acta 400 (2021), 139425.
[62] L. Han, H. Huang, J. Li, X. Zhang, Z. Yang, M. Xu, L. Pan, J. Mater. Chem .A 8 (2020) 15042–15050.
[63] L. Dong, X. Ma, Y. Li, L. Zhao, W. Liu, J. Cheng, C. Xu, B. Li, Q.-H. Yang, F. Kang, Energy Storage Mater. 13 (2018) 96–102.
[64] C.C. Hou, Y. Wang, L. Zou, M. Wang, H. Liu, Z. Liu, H.F. Wang, C. Li, Q. Xu, Adv. Mater. (2021), 2101698.
[65] W. Jian, W. Zhang, X. Wei, B. Wu, W. Liang, Y. Wu, J. Yin, K. Lu, Y. Chen, H.N. Alshareef, X. Qiu, Adv. Funct. Mater. 32 (2022), 2209914.
[66] Z. Xu, R. Ma, X. Wang, Energy Storage Mater. 46 (2022) 233–242.
[67] L. Wang, M. Peng, J. Chen, X. Tang, L. Li, T. Hu, K. Yuan, Y. Chen, ACS Nano 16 (2022) 2877–2888.

Please cite this article as: J. Li et al., Facile synthesis of accordion-like porous carbon from waste PET bottles-based MIL-53(Al) and its application for high-performance Zn-ion capacitor, Green Energy & Environment, https://doi.org/10.1016/j.gee.2023.01.002